S. D. Guest

S. Pellegrino

Department of Engineering,
University of Cambridge,
Trumpintgon Street,
Cambridge, CB2 1PZ, U.K.

The Folding of Triangulated Cylinders, Part II: The Folding Process

In the first paper of this series we have introduced a class of foldable triangulated cylinders. In this paper we consider three particular examples of these cylinders and analyse computationally the way they fold. We show that this process is nonuniform and that it consists of two phases. The first unsteady phase involves the gradual buildup of strain energy in a "shape transition region." In the second phase the transition region moves toward the bottom of the cylinder under almost zero force. Although the behavior of the three example cylinders is qualitatively similar, the peak force on the cylinder, as well as the peak strain, have different magnitudes, in agreement with a result in our first paper.

1 Introduction

In Guest and Pellegrino (1994), henceforth referred to as Part I, we have examined the folding properties of triangulated cylinders like that shown in Fig. 1. By considering a uniform folding mode, which is a simplification of the mode observed in physical experiments, we obtained preliminary estimates of the strains imposed on a triangulated cylinder during folding. In this paper we restrict our attention to a particular type of cylinder which, in terms of the geometric parameters introduced in Part I, have $m = 1$ and $l_b/l_a = 1$ and hence can be packaged "flat" into prismatic stacks of plates. We consider three cylinders of this type, with $n = 6, 7$, and 8, and analyze computationally the way they fold when pressed down by a flat plate. Our prime interest, of course, is in the level of straining induced by this process and also the force required to fold a cylinder. We are also interested in the shape of the transition region immediately ahead of the fully packaged region, and the decay pattern of the strain field. Such information is needed for the design, manufacture, and testing of foldable cylinders. Indeed, only after obtaining some preliminary results of the investigation reported in this paper was it possible to manufacture the Al-alloy cylinder which is shown in Fig. 1 of Part I.

In the next section we set out our computational approach which can handle the inextensional mechanisms present at the end of a triangulated cylinder (activated only during the early stages of folding), and also the variable boundary conditions due to the unilateral support conditions imposed by the loading
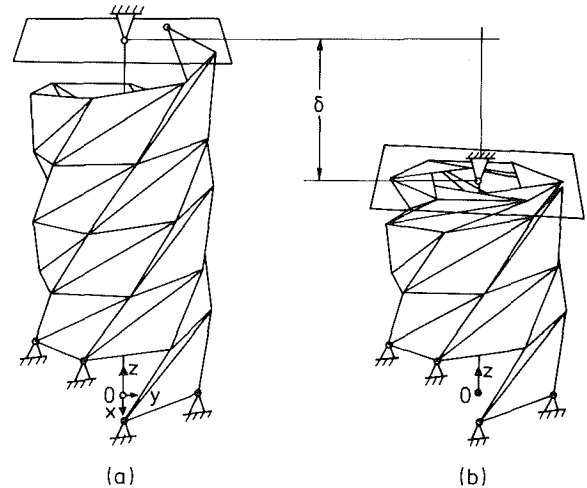
Fig. 1 Triangulated cylinder with $m = 1$, $n = 7$, $l_b/l_a = 1$, and $l_c/l_a = \sqrt{3}$, folded by moving down a rigid plate; (a) fully extended configuration, $k = 1$; (b) partially folded configuration, $k = 12$. The bottom n nodes of the cylinder are fully restrained. The coordinate system O, x, y, z has the z-axis aligned with the axis of the cylinder; the bottom node lies in the x-y plane.

plate. Then, in Section 3 we present and discuss the results obtained for a cylinder with $n = 7$, which folds down to a hexagonal prism, and compare its response to that of cylinders with $n = 6$ and $n = 8$: all cylinders have $m = 1$ and $l_b/l_a = 1$. Although the folding process is fundamentally the same for all of them, it turns out that the peak strains, the peak force on the loading plate, etc., tend to become smaller as n increases.[1]

___
[1]A number of cylinders have now been tested. Many features of their behavior agree with the results presented here, but some other interesting features have also emerged. They will be discussed in a third paper in this series.

Fig. 2 (a) Forces acting on the top plate; (b) the corresponding forces on the top k nodes of the cylinder

2 The Algorithm

A simple analytical model of a triangulated cylinder is a truss structure having linear elastic bars of equal cross-section along the edges of the triangles and connected at the nodes by frictionless pin-joints. There are three types of bars, a, b, c, lying on the edges labeled thus in Fig. 3 of Part I. The bottom n nodes of the structure are fully fixed. The structure is compressed by a frictionless, rigid plate which is connected to a rigid foundation at a single point. To simulate the folding process, this point is gradually drawn towards the bottom end of the structure. For simplicity, the thickness of the triangular plates making up the cylinder is neglected.

This model can capture key aspects of the folding process, such as the formation of a shape transition region under gradually increasing force, and its propagation under constant force, which have been observed experimentally. It is also useful to make comparisons between triangulated cylinders with different parameters.

The algorithm presented here is based on a Force Method approach, hence it requires that the overall equilibrium, compatibility, and flexibility matrices be available for any given configuration of the cylinder. These matrices are obtained by assembling the basic matrices of two types of elements, the pin-jointed bars and the rigid loading plate. Of course, there is no difficulty in setting up the matrices for a pin-jointed bar (Livesley, 1975). But the loading plate is not a standard element and we shall briefly explain how to set up the three matrices required, in the hypothesis that all forces acting on the loading plate are orthogonal to it.

Let us consider the loading plate shown in Fig. 2(a), whose current configuration is defined by the position of point P and by the unit normal vector $\mathbf{u}$. The plate is acted upon by k interaction forces between the plate and the k joints of the cylinder in contact with it. Equal and opposite forces act upon the top k joints of the cylinder, as shown in Fig. 2(b). The plate is also acted upon by a force of magnitude R and a couple of magnitude Q, applied to it by the foundation through the connecting hinge at P. All of these forces, as well as the vector representing Q, are orthogonal to the plate, i.e., parallel to $\mathbf{u}$. In addition to point P, let us define k points on the plate, P_1, $\ldots$, P_k; an interaction force of magnitude R_i passes through point P_i. Only compressive R_i's—i.e., opposite to those shown in Fig. 2—are physically meaningful and, although no restrictions on their sign will be imposed in this study, this is a point worth considering in future work.

Although, in general, there are six independent equations of equilibrium for a rigid body, in this particular case—because the plate is under the action of a system of parallel forces—two equations of force equilibrium are identically satisfied. Hence, we need to consider only the equilibrium of forces in the u-direction, which yields the matrix equation

$$[1 \ \ldots \ 1 \ 1] \begin{bmatrix} R_1 \\ \cdots \\ R_k \\ R \end{bmatrix} = 0 \qquad (1)$$

and the equilibrium of moments about any point. Because of the kinematic implications of these equations (see below) it is easiest to take moments about a set of axes parallel to x, y, and z (defined in Fig. 2(b)) and passing through P. The three moment components of the interaction force at P_i are $(P_i - P) \times (-\mathbf{u})R_i$, hence the three equations of moment equilibrium for the plate can be written in the form

$$[(P_1-P) \times \mathbf{u} \ \ldots \ (P_k-P) \times \mathbf{u} \ \mathbf{u}] \begin{bmatrix} R_1 \\ \cdots \\ R_k \\ Q \end{bmatrix} = \begin{bmatrix} 0 \\ 0 \\ 0 \end{bmatrix}. \qquad (2)$$

The r.h.s. of Eq. (1) and (2) have been set directly equal to zero because there are no external forces acting on the plate. Note that the reactions R and Q have been put among the internal forces because their values are not known a priori.

By assembling together Eqs. (1) and (2) we obtain a system of four equations in $k + 2$ generalized stresses, whose 4 by $k + 2$ coefficient matrix is the equilibrium matrix $\mathbf{A}_p$ for the plate:

$$\begin{bmatrix} 1 & \ldots & 1 & 1 & 0 \\ & & & & 0 \\ (P_1-P) \times \mathbf{u} & \ldots & (P_k-P) \times \mathbf{u} & 0 & \mathbf{u} \\ & & & & 0 \end{bmatrix} \begin{bmatrix} R_1 \\ \cdots \\ R_k \\ R \\ Q \end{bmatrix} = \begin{bmatrix} 0 \\ 0 \\ 0 \\ 0 \end{bmatrix}. \qquad (3)$$

The transpose of $\mathbf{A}_p$ relates the kinematic variables corresponding to the static variables in Eq. (3) (Livesley, 1975). The $k + 2$ generalized strains, corresponding to the vector on the l.h.s. of Eq. (3), are the extensions e_i of the "connectors" between the plate and the top k joints of the cylinder, together with the u-displacement of point P, d_{Pu}, and the plate rotation ϕ about the u-axis. The four generalized displacements are d_{Pu}, α, β, γ. The variable d_{Pu} appears both as internal and external and so it should be no surprise that the corresponding kinematic equation is a simple identity. The variables α, β, γ are the small rotations of the plate about the x, y, and z-axis, respectively. The system of kinematic equations is

$$\begin{bmatrix} 1 & (P_1-P) \times \mathbf{u} \\ \cdots & \cdots \\ 1 & (P_k-P) \times \mathbf{u} \\ 1 & 0 \quad 0 \quad 0 \\ 0 & \mathbf{u} \end{bmatrix} \begin{bmatrix} d_{Pu} \\ \alpha \\ \beta \\ \gamma \end{bmatrix} = \begin{bmatrix} e_1 \\ \cdots \\ e_k \\ d_{Pu} \\ \phi \end{bmatrix} \qquad (4)$$

The third matrix is straightforward: because the plate and its foundation are rigid all entries in the $k + 2$ by $k + 2$ flexibility matrix $\mathbf{F}_p$ must be zero.

Note that the above formulation, with four external variables, is not the most compact, only two variables are really needed. The size of all three matrices for the plate could be reduced by two rows and two columns, at the expense of a few extra computations.

The matrices derived above are assembled together with the matrices for the pin-jointed bars to form the overall matrices for the cylinder. Let N be the total number of nodes in the cylinder and B the total number of bars. Because the bottom n nodes are fully fixed to a rigid foundation, the corresponding $3n$ equilibrium equations need not be considered. At the top of the cylinder the k nodes in contact with the rigid plate do

not need any special treatment, apart from noting that each of these joints is subject to an interaction force of magnitude R_i, as shown in Fig. 2(b), as well as to the axial forces in the bars connected to it. Hence, there are $3(N - n) + 4$ equilibrium equations in $B + k + 2$ generalized stresses σ and the overall equilibrium matrix $\mathbf{A}$ has size $3(N - n) + 4$ by $B + k + 2$. Similarly, the generalized strain vector ϵ has size $B + k + 2$, while the generalized displacement vector $\mathbf{d}$ has size $3(N - n) + 4$; the flexibility matrix $\mathbf{F}$ has size $B + k + 2$ by $B + k + 2$.

With these tools, the folding of a triangulated cylinder can be analyzed. One begins by setting up the cylinder in its fully extended configuration (as in Section 2 of Part I but w.r.t. the Cartesian coordinate system defined in Fig. 1(a)). The loading plate is set initially parallel to the x-y plane and the connection point P has coordinates $P = (0, 0, z_p)$, where z_P is also the z-coordinate of the top node of the cylinder. Obviously, at the beginning this is the only node which is in contact with the loading plate, hence $k = 1$.

To compute the folding sequence, the value of z_P is decreased in small steps; note that δ, the overall shortening of the cylinder, see Fig. 1(b), is equal to the difference between the initial z_P and its current value. In each step the starting configuration is based on the shape of the cylinder computed at the end of the previous step, only z_P is changed. Obviously, this imposes some strains in the k connectors between the plate and the cylinder and, because they are rigid, these strains must be relieved through suitable displacements. Note that, with this approach, the folding of the cylinder is achieved simply by moving one of its boundaries, i.e., without applying any external forces (the force on the loading plate is treated as an internal force, thus simulating a *displacement controlled test*). If the imposed strains are compatible they produce, of course, only a displacement from the current configuration. This is always the case at the beginning of the folding process and, indeed, at this point the configuration of the loading plate is not uniquely defined. In our simulations, a unique configuration is selected by minimizing the generalized displacement. In general, though, the imposed strains have an incompatible component which sets up a state of self-stress in the system. The calculation of the effects of these strains is geometrically nonlinear because (i) the plate is free to rotate about any in-plane axis (although no u-rotation is allowed), and (ii) it is fairly sensitive to small geometry changes. A further source of nonlinearity is the variability of k, discussed below.

For each value of z_P, our algorithm performs a series of Newton-Raphson iterations to find the new shape of the cylinder and the corresponding value of R. Initially, the displacement $\mathbf{d}^0$ from the current configuration is set to zero and the initial strain $\Delta\epsilon_o$ involves strains in the k connectors only. In iteration i, the system is in the trial configuration defined by $\mathbf{d}^{i-1}$. The strains $\Delta\epsilon_o$ are given, for the bars, by the difference between current trial length and initial, unstrained length. The extensions of the k plate-cylinder connectors are equal to the distance between the top k joints and the loading plate. The overall equilibrium matrix $\mathbf{A}^i$ is formed in this configuration and, after computing the Singular Value Decomposition of $\mathbf{A}^i$, the stresses $\Delta\sigma$ and displacements $\Delta\mathbf{d}$ induced by $\Delta\epsilon_o$ are found (Pellegrino, 1993). Finally, a new trial configuration is obtained from

$$\mathbf{d}^i = \mathbf{d}^{i-1} + \Delta\mathbf{d}.$$

The iteration stops when $\Delta\mathbf{d}$ is sufficiently small. If any nodes of the cylinder have gone past the plate, k is incremented by 1 and a new series of Newton-Raphson iterations is started. Finally, the shape of the cylinder is updated.

3 Simulation of the Folding Process

Let us consider the triangulated cylinder shown in Fig. 1(a). It has $m = 1$, $n = 7$, $l_b/l_a = 1$, and $l_c/l_a = \sqrt{3}$. According to Part 1, an unrestrained cylinder with these parameters has two strain-free configurations: one fully folded, the other fully extended. Figure 1(a) shows the fully extended configuration.

This cylinder will be modelled as a pin-jointed truss, as discussed in Section 2: the total numbers of joints and bars are $N = 36$ and $B = 86$; bars joining two fully restrained nodes have been taken out. All bars have equal axial stiffness AE. In the extended configuration node 1 (at the bottom of the cylinder) has $z = 0$, while node 36 (at the top of the cylinder) has $z = 4.175 \, l_a$. The bottom $n = 7$ nodes are fully restrained: the z-coordinate of the last restrained node is $0.716 \, l_a$. Clearly the folding of the cylinder cannot go past this point. The rigid plate at the top of the cylinder is set initially in contact with node 36, hence $z_P = 4.175 \, l_a$ and $k = 1$. At this stage $\delta = 0$. Starting from this configuration we have lowered the plate by decreasing z_P in steps of $l_a/100$.

Results from a simulation involving approximately 300 steps are shown in Figs. 3-4. Figure 3(a) shows dimensionless plots of the force R and the strain energy U in the cylinder. The cylinder begins to fold under zero force, hence remaining strain-free, until $k = 4$. Then R starts increasing until, when $k = 8$, it reaches a peak and then falls off. Subsequently, R periodically oscillates around zero. The strain energy increases considerably when k goes from 3 to 9, but then remains approximately constant. In fact the strain energy plots show a slow increase, due to end effects in the top part of the cylinder, since the fully folded region does not yet contain enough bars to allow the natural decay of strain to take place.

Fig. 3(b) shows some more details of the steady state regime; the periodic variation of R is directly related to changes in k. R is negative, i.e., tensile, just before a new node comes into contact with the plate and there is a sudden stiffness increase caused by the activation of an extra constraint, which corresponds to an increment in the value of k. As δ is increased, R increases until a limit point, it then decreases until the beginning of a new cycle. Note that in our simulation R is negative at the beginning and at the end of a cycle, which is unrealistic. In practice, a small spring-back of the folded region is likely to occur.

The folding cylinder is a continuously softening system, with

$$\frac{d^2 R}{d\delta^2} < 0$$

wherever this quantity is defined, but the system is periodically stiffened as new nodes come into contact with the top plate. Although unusual, this behavior has some similarities to the axial crushing of cellular materials (Gibson and Ashby, 1988).

Next, we look at strain variation during steady-state folding. For a clear picture of strain distribution it is best to consider the axial strain ϵ_c in the 28 c bars, plotted in Fig. 3(c). As the plate is pushed down, the most significant part of the strain field, say $\epsilon_c > 10^{-3}$, simply translates from right to left, i.e., from the top towards the bottom of the cylinder. However, a region involving compressive strains gradually builds up in the wake of the shape-transition region and the strain energy associated with it is responsible for the slow strain energy increase discussed earlier.

The most significant feature of Fig. 3(c) is the peak strain attained: here $\epsilon_{c\,max} = 8.7 \cdot 10^{-3}$. Similar plots are obtained for the a and b bars, whose (compressive) peak strains are $5.0 \cdot 10^{-3}$ and $6.9 \cdot 10^{-3}$, respectively.

Figure 3(d) shows strain plots, again for the c bars only, (i) just after a node has come into contact with the plate, (ii) when R reaches its peak, and (iii) just before a new mode comes into contact with the plate. Here, $k = 14$ throughout. Note that the peak strain remains essentially unchanged during this cycle.

Figure 3(e) shows the orientation of the loading plate by means of plots of the x, y, and z-components of $\mathbf{u}$. The plate normal essentially describes a small conical motion about the
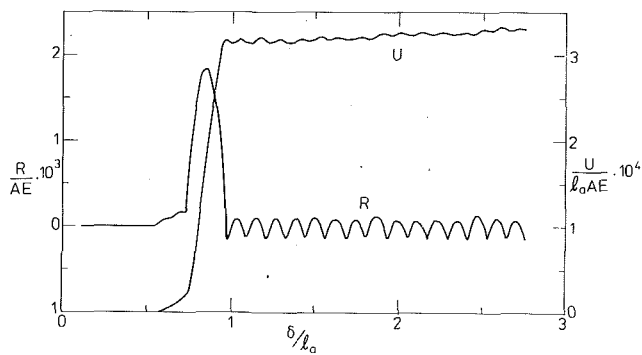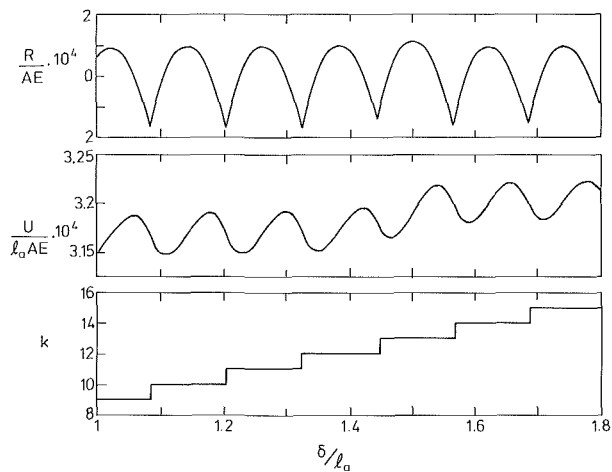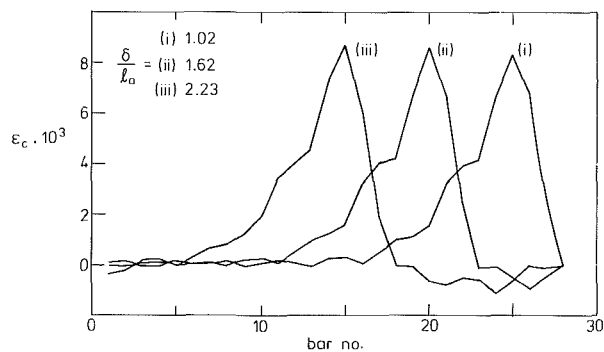
Fig. 3(a)

Fig. 3(b)
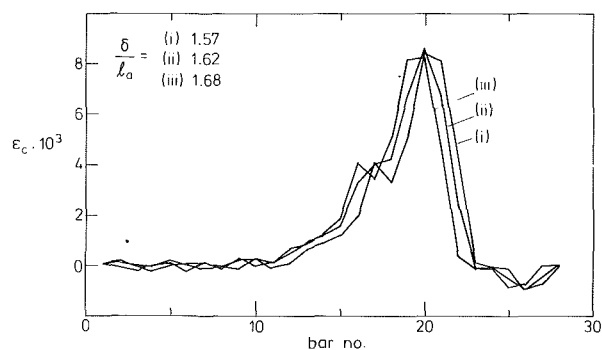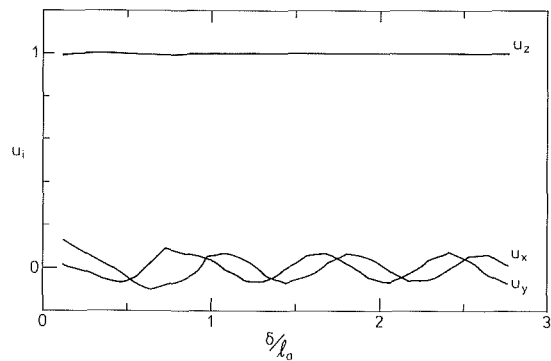

Fig. 3(c)

Fig. 3(d)

Fig. 3(e)

Fig. 3 Folding of cylinders with $m = 1$, $n = 7$, $l_b/l_a = 1$, and $l_c/l_a = \sqrt{3}$; (a) plots of R and U in the cylinder; (b) detailed data for steady-state phase; (c, d) ϵ_c during steady-state folding. Bars take the number of their bottom node, and nodes are numbered going up on the a helix. Discrete values have been joined, for legibility; (e) three components of u.

Fig. 4 Fully extended view of cylinder with $m = 1$, $n = 7$, $l_b/l_a = 1$, and $l_c/l_a = \sqrt{3}$, followed by three snapshots from the folding sequence

z-axis. Figure 4 shows four snapshots from the simulation process, including the initial configuration.

Next, we compare the behavior of the three cylinders shown in Fig. 2 of Part I, to gain further insight into the folding process. One of them is the triangulated cylinder examined above, with $m = 1$, $n = 7$, $l_b/l_a = 1$, and $l_c/l_a = \sqrt{3}$. The two other cylinders also have $m = 1$ and $l_b/l_a = 1$: the first has $n = 6$ and $l_c/l_a = 1.618$; the second has $n = 8$ and $l_c/l_a = 1.802$.

The folding of these two cylinders has been analyzed by the technique described above. For $n = 6$ we have considered a pin-jointed truss with $N = 31$ and $B = 74$. In the fully extended configuration $z_P = 4.912\ l_a$. To initiate the correct folding pattern, the simulation had to start with three nodes in contact with the plate. If a smaller number is chosen, the top plates start folding outwards and quickly the process comes to halt. Figure 5(a) shows plots of the force R and of the strain energy U. As for $n = 7$, there is a large force peak and a corresponding increase in strain energy soon after the beginning of the process;

afterwards, R oscillates around zero and U remains approximately constant. Figure 5(b) shows the strain field in the c bars; as in Fig. 3(c) the most significant part of the strain field simply translates from right to left. Qualitatively these results are the same as for the earlier cylinder, but the key difference between the cases $n = 6$ and $n = 7$ is in the magnitudes of forces and strains: R_{max} and $\epsilon_{c\,max}$ are, respectively, 14 and 4 times higher for $n = 6$ than for $n = 7$.

For the case $n = 8$ we have considered a pin-jointed truss with $N = 49$ and $B = 122$ which, when fully extended, has $z_P = 2.818\ l_a$. Starting from this position the plate has been lowered gradually: the folding behavior of this cylinder, see Fig. 6, is essentially identical to the earlier cases. Note that the trend towards lower forces and strains continues: R_{max} and $\epsilon_{c\,max}$ are, respectively, 150 and 17 times higher for $n = 7$ than for $n = 8$. The complete set of values is available in Table 1.
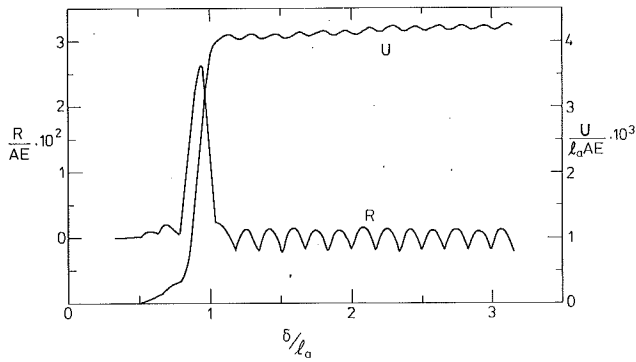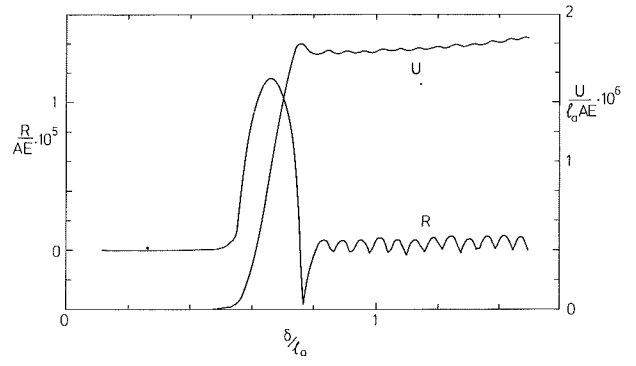
Journal of Applied Mechanics
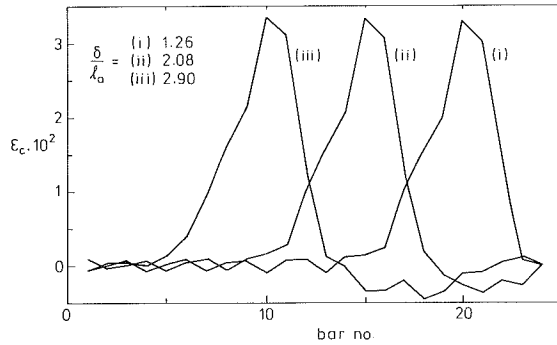
Fig. 5(a)

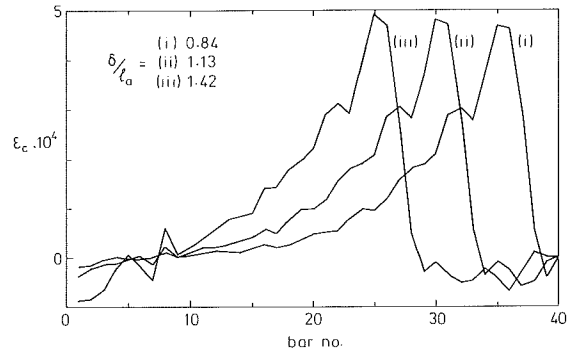**Fig. 6(a)**

Fig. 5(b)

Fig. 6(b)

Fig. 5 Folding of cylinders with $m = 1$, $n = 6$, $l_b/l_a = 1$, and $l_c/l_a = 1.618$

Fig. 6 Folding of cylinders with $m = 1$, $n = 8$, $l_b/l_a = 1$, and $l_c/l_a = 1.802$

4 Discussion

Before discussing the results obtained in this paper it is necessary to comment on the validity of the assumptions behind our approach, namely that a triangulated cylinder can be modeled as a simple pin-jointed truss and that plate thickness can be neglected. Although more complex models could be considered, we think that it would be pointless to do this in a purely conceptual study. More detailed models would need to be firmly based on the mechanical features of a particular triangulated cylinder. For example, in the model shown in Fig. 1 of Part I the plates are connected by thin plastic links which are very flexible in comparison with the plates, and the deformation of such a system is concentrated in these connections. If, on the other hand, more traditional mechanical hinges are used, the effects of joint tolerance would have to be considered. Finally, the pin-jointed truss model assumes that the connections between plates offer no resistance to bending. If this is not the case there would have to be a larger strain energy increase during folding, but we do not expect higher peak strains. Regarding the second assumption, we expect that plate thickness does not play a significant role because its effects do not accumulate in this case unlike, e.g., the wrapping of a membrane around a central hub (Guest and Pellegrino, 1992).

The simulations presented in Section 3 have revealed that the folding of a triangulated cylinder consists of two phases. The first unsteady phase involves a gradual buildup of strain energy under a large applied force, which might provide an effective self-locking feature. During this phase a shape transition region from the fully extended to the fully folded part of the cylinder is formed and, once the energy barrier that prevents folding has been overcome, a second steady-state phase of the process begins. During this phase the shape transition region moves towards the bottom of the cylinder under almost zero force. These observations agree qualitatively with

Table 1 ϵ_{max} and R_{max} in cylinders with $m = 1$ and $l_b/l_a = 1$

n	$|\epsilon_a|_{max}$	$|\epsilon_b|_{max}$	$|\epsilon_c|_{max}$	R_{max}/AE
6	$2.0 \cdot 10^{-2}$	$2.7 \cdot 10^{-2}$	$3.6 \cdot 10^{-2}$	$2.6 \cdot 10^{-2}$
7	$5.0 \cdot 10^{-3}$	$6.9 \cdot 10^{-3}$	$8.7 \cdot 10^{-3}$	$1.8 \cdot 10^{-3}$
8	$3.5 \cdot 10^{-4}$	$4.1 \cdot 10^{-4}$	$5.2 \cdot 10^{-4}$	$1.2 \cdot 10^{-5}$

the behavior of several models, including that shown in Fig. 1 of Part I and many card models.

In the three cylinders which have been analyzed in this paper both the peak force and peak strain decrease rapidly as n increases, as noted in Section 3, but the role played by this particular parameter should not be overvalued. The aim of the present study was a characterization of the general folding behavior of triangulated cylinders for which we selected three cylinders that fold down to simple prisms. Although a detailed investigation of design parameters is beyond the scope of the present investigation, it can be noted that the key factor determining peak force and peak strain is the size of the geometric incompatibility shown in, e.g., Fig. 6 of Part I. The particular combination of the parameters m, n, l_b/l_a, and l_c/l_a which leads to it is not very significant. Thus, for example, a similar range of ϵ_{max} and R_{max} to that obtained here, for $n = 6, 7, 8$ but $m = 1$ and $l_b/l_a = 1$, could be obtained with constant n, by varying l_b/l_a.

Finally, it is interesting to compare the present simulations of the folding process with the approach pursued in Part I. A comparison has been made in Table 2 for the case $m = 1$, $n = 7$, $l_b/l_a = 1$, and $l_c/l_a = \sqrt{3}$. The table gives also "modified" peak strains, estimated in the spirit of Part I but allowing all bar lengths to vary simultaneously with constant ratios l_c/l_a and l_b/l_a. Note that these simplified estimates are higher than

Table 2 Comparison of predictions in Part I and Part II, for cylinders with $m = 1$, $n = 7$, $l_b/l_a = 1$, and $l_c/l_a = \sqrt{3}$

	$|\varepsilon_a|_{max}$	$|\varepsilon_b|_{max}$	$|\varepsilon_c|_{max}$
Part 1	0	0	$2.5 \cdot 10^{-2}$
Part 1 (modified)	$1.2 \cdot 10^{-2}$	$1.2 \cdot 10^{-2}$	$1.3 \cdot 10^{-2}$
Part 2	$5.0 \cdot 10^{-3}$	$6.9 \cdot 10^{-3}$	$8.7 \cdot 10^{-3}$

the predictions obtained with the present method, hence "safe" for preliminary design of foldable cylinders.

Acknowledgments

References

Gibson, L. J., and Ashby, M. F., 1988, *Cellular Solids: Structure & Properties*, Pergamon Press, Oxford, U.K.

Guest, S. D., and Pellegrino, S., 1992, "Inextensional Wrapping of Flat Membranes," *Proc. First International Seminar on Structural Morphology*, R. Motro, ed., Montpellier, La Grand Motte, Sept. 7–11, pp. 203–215.

Guest, S. D., and Pellegrino, S., 1994, "The Folding of Triangulated Cylinders, Part I: Geometric Considerations," ASME JOURNAL OF APPLIED MECHANICS, Vol. 61, pp. 773–777.

Livesley, R. K., 1975, *Matrix Methods of Structural Analysis*, 2nd ed., Pergamon Press, Oxford, U.K.

Pellegrino, S., 1993, "Structural Computations with the Singular Value Decomposition of the Equilibrium Matrix," *International Journal of Solids and Structures*, Vol. 30, pp. 3025–3035.